

**UNCLASSIFIED**

**Defense Technical Information Center  
Compilation Part Notice**

**ADP012598**

**TITLE:** Quantum Dot Long-Wavelength Detectors

**DISTRIBUTION:** Approved for public release, distribution unlimited

This paper is part of the following report:

**TITLE:** Progress in Semiconductor Materials for Optoelectronic Applications Symposium held in Boston, Massachusetts on November 26-29, 2001.

To order the complete compilation report, use: ADA405047

The component part is provided here to allow users access to individually authored sections of proceedings, annals, symposia, etc. However, the component should be considered within the context of the overall compilation report and not as a stand-alone technical report.

The following component part numbers comprise the compilation report:

ADP012585 thru ADP012685

**UNCLASSIFIED**

## Quantum Dot Long-Wavelength Detectors

Pallab Bhattacharya, Adrienne D. Stiff-Roberts, Sanjay Krishna<sup>1</sup>, and Steve Kennerly<sup>2</sup>  
Solid State Electronics Laboratory, Department of Electrical Engineering and Computer  
Science, University of Michigan  
Ann Arbor, MI 48109-2122, U.S.A.

<sup>1</sup>Center for High Technology Materials, Department of Electrical Engineering and  
Computer Engineering, University of New Mexico  
Albuquerque, NM 87106, U.S.A.

<sup>2</sup>Sensors and Electron Devices Directorate, U. S. Army Research Laboratory  
Adelphi, MD 20783, U.S.A.

### ABSTRACT

Long-wavelength infrared detectors operating at elevated temperatures are critical for imaging applications. InAs/GaAs quantum dots are an important material for the design and fabrication of high-temperature infrared photodetectors. Quantum dot infrared photodetectors allow normal-incidence operation, in addition to low dark currents and multispectral response. The long intersubband relaxation time of electrons in quantum dots improves the responsivity of the detectors, contributing to better high-temperature performance. We have obtained extremely low dark currents ( $I_{dark} = 1.7 \text{ pA}$ ,  $T = 100 \text{ K}$ ,  $V_{bias} = 0.1 \text{ V}$ ), high detectivities ( $D^* = 2.9 \times 10^8 \text{ cmHz}^{1/2}/\text{W}$ ,  $T = 100 \text{ K}$ ,  $V_{bias} = 0.2 \text{ V}$ ), and high operating temperatures ( $T = 150 \text{ K}$ ) for these quantum-dot detectors. These results, as well as infrared imaging with QDIPs, will be described and discussed.

### INTRODUCTION

Infrared detection is important in a variety of fields, such as military targeting and tracking, law enforcement, environmental monitoring, and space science. Quantum dot infrared photodetectors (QDIPs) have been widely investigated during the past few years for operation in the mid-wavelength (3-5  $\mu\text{m}$ ) and long-wavelength (8-14  $\mu\text{m}$ ) infrared ranges [1-13]. Three of the major advantages expected from QDIPs over other existing technologies are; (i) normal incidence operation, eliminating the need for external gratings and optocouplers [5,8,10], (ii) high-temperature operation, eliminating the need for expensive cooling systems presently used with mercury cadmium telluride (MCT) detectors [14,15] and quantum well infrared photodetectors (QWIPs) [16,17], and (iii) decreased dark current, increasing the background-limited performance (BLIP) of the detector. Since InAs/GaAs quantum dots are grown by molecular beam epitaxy (MBE) using the mature III-V technology, they are essentially defect-free and do not suffer from the etch-pit densities and void defects that plague MCT detectors. The main disadvantage of the QDIP is the large inhomogeneous linewidth of the quantum dot ensemble due to random variation of dot size in the Stranski-Krastanow growth mode.

Despite such challenges, QDIPs are expected to perform better at higher temperatures, especially when compared to QWIPs, due to the increased intersubband relaxation time between the phonon-decoupled ground state and excited states, increasing

the probability that a photoexcited carrier will be collected as photocurrent [9,18-20]. This long intersubband relaxation time in quantum dots results from the existence of a “phonon bottleneck” that prevents electron relaxation by a single phonon emission. Such single phonon processes dominate carrier scattering and relaxation in quantum wells, resulting in relaxation times  $\sim$  2-5 ps [21]. Since, intersubband relaxation in quantum dots occurs by a multi-phonon event, which requires the satisfaction of a stringent resonant condition, this process is very slow ( $>1$  ns). Differential transmission spectroscopy (DTS) [20,22] and high-frequency electrical impedance (HFEI) measurements [21] on  $\text{In}_{0.4}\text{Ga}_{0.6}\text{As}/\text{GaAs}$  quantum dots and quantum dot laser diodes, respectively, have revealed the following picture of hot-carrier dynamics in the conduction band of quantum dots, depicted in figure 1. Electrons relax from the barrier to the excited state in 1-2 ps. Electron relaxation from the excited state to the ground state exhibits two time constants: (i) a short time constant ( $\sim$  6-8 ps), due to Auger-like processes, intradot electron-hole scattering, and multi-phonon emission [23]; and (ii) a long time constant ( $\sim$  15-100 ps), depending on the temperature and excitation level, which is phonon-mediated and demonstrates the phonon-bottleneck phenomenon. These studies also demonstrate that the faster relaxation is a geminate process, wherein the injected electron and hole are captured in the same dot, whereas the slow relaxation process is a non-geminate process, wherein the injected electrons and holes are captured in separate dots, by virtue of the sample temperature or scattering processes. Similar characteristics with respect to long intersubband relaxation times are expected to exist in other III-V quantum dots, such as the InAs/GaAs quantum dots used in QDIPs.

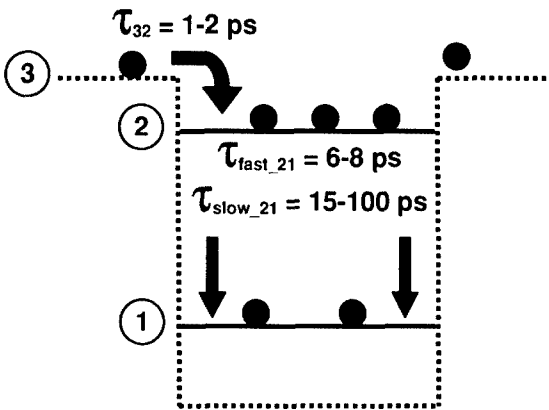


**Figure 1.** Schematic depiction of electron relaxation times in the conduction band of  $\text{In}_{0.4}\text{Ga}_{0.6}\text{As}/\text{GaAs}$  quantum dots. The long intersubband relaxation time from level 2 to level 1 is responsible for many of the expected advantages of QDIPs.

## EXPERIMENTAL DETAILS

The InAs/GaAs quantum dots comprising the active region of the vertical QDIPs were grown by solid source molecular beam epitaxy (MBE) using a Varian GEN-II machine with an uncracked As<sub>4</sub> source. Several generations of the device were characterized before obtaining the current best performing detector. The different conduction band profiles for these trial heterostructures are shown in figure 2(a). The results shared in this paper are for the vertical QDIP with a single 30% AlGaAs barrier at the top of ten InAs/GaAs quantum dot layers. First, a 0.5 μm silicon-doped ( $n = 2 \times 10^{18} \text{ cm}^{-3}$ ) GaAs contact layer was deposited on a semi-insulating (100) GaAs substrate at a growth temperature of 620 °C. Next, a 250 Å intrinsic GaAs buffer was grown. The substrate temperature was decreased to 500 °C, and 2.2 ML of InAs were deposited to form the quantum dots. The reflection high-energy electron diffraction (RHEED) pattern was monitored during growth of the dots in order to observe the transition from a layer-by-layer to an island growth mode after about 1.7 ML of InAs deposition. A 250 Å intrinsic GaAs cap layer was grown on top of the InAs in order to complete the quantum dot barrier. This sequence of growth was then repeated nine times for a ten-layer InAs/GaAs quantum dot active region. After the final GaAs layer was grown, the substrate temperature was increased to 620 °C, and 400 Å of intrinsic Al<sub>0.3</sub>Ga<sub>0.7</sub>As were deposited in order to form a current-blocking barrier at the top of the device. Finally, a 0.1 μm silicon-doped ( $n = 2 \times 10^{18} \text{ cm}^{-3}$ ) GaAs top contact layer was grown.

A standard, three-step photolithography and wet-etching technique was used to fabricate the device. The first step comprised Ni/Ge/Au/Ti/Au metal evaporation for the top ring contact. Next, a mesa etch ( $\approx 1 \mu\text{m}$ ) was performed around the top contact to define the active region for a single pixel. Finally, the metal evaporation was repeated for the bottom ring contact, which was deposited around the device mesa. The device was annealed at 400 °C for approximately one minute in order to make ohmic contacts. An SEM micrograph of a fabricated device is shown in figure 2(b).

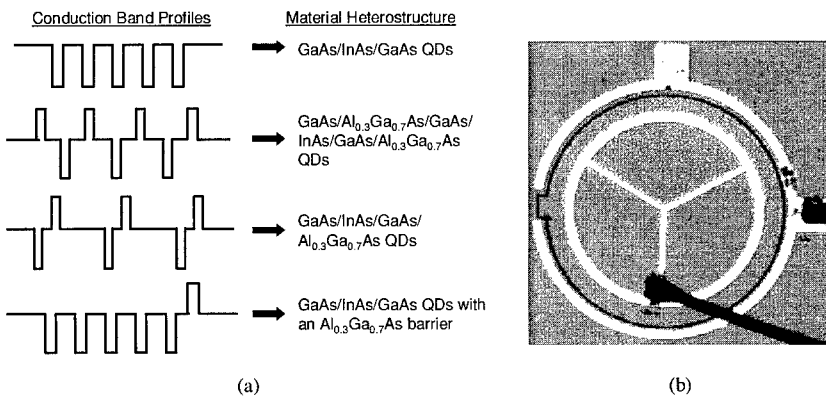


**Figure 2.** (a) Conduction band profiles for various vertical QDIP heterostructures; and (b) SEM micrograph of a fabricated vertical QDIP with an optical area of  $2.83 \times 105 \text{ mm}^2$ .

## RESULTS AND DISCUSSION

Several measurements were conducted in order to completely characterize the vertical QDIP; namely, dark current, spectral response, noise spectra/blackbody response, and dark current uniformity measurements. These characteristics have been discussed in detail previously [24,25]. In the vertical device, at a detector temperature of 100 K, the dark current was 1.7 pA at a bias voltage of 0.1 V, which is an extremely low value. It is evident that the 30% AlGaAs barrier in the vertical QDIP successfully blocks dark current, as shown in figure 3(a), yielding lower dark currents than many other IR detectors. The spectral response was obtained for a detector temperature of 78 K in the vertical QDIP. The  $\lambda_{\text{peak}}$  for the response of the vertical QDIP, is 3.72  $\mu\text{m}$ , and  $\Delta\lambda/\lambda$  is 0.3, indicating a bound-to-continuum transition [5]. An 800 K blackbody source was used to calibrate the absolute responsivity of the QDIP to normally incident IR radiation for the noise spectra and blackbody response measurements. A germanium block was used at the shutter of the blackbody source in order to filter out near-IR radiation (< 1.8  $\mu\text{m}$ ) emitted by the blackbody. The vertical QDIP was characterized at 78 K, 100 K, 125 K and 150 K, and the best device performance was measured at 100 K. The maximum  $R_{\text{peak}}$  value of 2 mA/W for a bias of 0.3 V at 100 K is relatively low when compared to MCT detectors or QWIPs. The low responsivity results from the AlGaAs barrier, which not only blocks dark current, but the photocurrent as well. Despite the low  $R_{\text{peak}}$ , due to the low noise floor in the devices, a maximum  $D^*$  of  $2.94 \times 10^9 \text{ cmHz}^{1/2}/\text{W}$  at a bias of 0.2 V is obtained at 100 K, which is a significant milestone in the performance of normal-incidence, vertical QDIPs. The responsivity and detectivity are shown in figure 3(b). Another important result is that the normal-incidence, vertical QDIP could be characterized up to a temperature as high as 150 K before the dark current exceeded the photocurrent, resulting in a signal-to-noise ratio less than one.

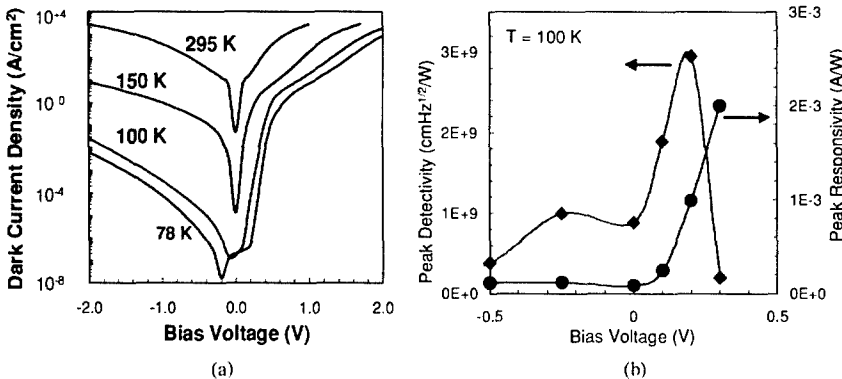


**Figure 3.** (a) Dark current density ( $\text{A}/\text{cm}^2$ ) and (b) peak responsivity and detectivity as a function of bias voltage for InAs/GaAs vertical QDIPs with a 30% AlGaAs barrier.

The encouraging performance characteristics of discrete QDIPs motivated us to explore their application to imaging arrays. The low-bias performance and simple device structure of the vertical QDIP make it the most readily adaptable device to currently available silicon read-out circuits for the fabrication of focal plane arrays. An important factor in the success of a focal plane array is the pixel operability, which depends greatly on the uniformity of a detector array. As a preliminary study, we considered the uniformity of dark current I-V curves at room temperature across a 4x4 vertical QDIP array. The mesa size was 50  $\mu\text{m}$  and the pitch was 100  $\mu\text{m}$ . An SEM micrograph of the fabricated array is shown in figure 4(a). As shown in the bubble diagram of figure 4(b), the dark current is fairly consistent across the array. The size of the bubble represents the magnitude of the dark current at the different pixel positions, and there is not a great variation across the array. This signifies that even though quantum dots do suffer from large inhomogeneous linewidths due to the random Stranski-Krastanow growth mode, vertical QDIPs still possess enough uniformity to make feasible the fabrication of large-area focal plane arrays.

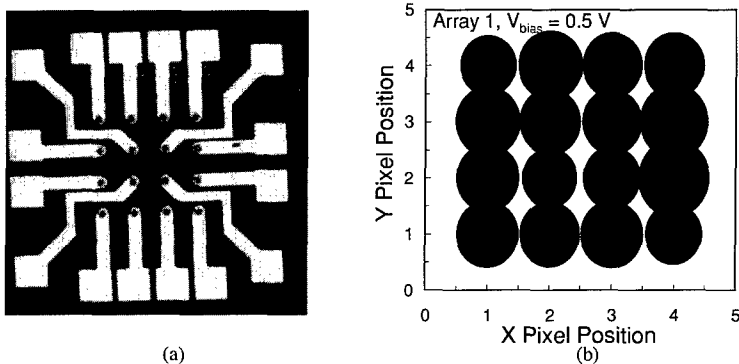


**Figure 4.** (a) SEM micrograph of fabricated 4x4 vertical QDIP array with 50  $\mu\text{m}$  mesa size and 100  $\mu\text{m}$  pitch; and (b) bubble diagram of dark current magnitude as a function of pixel position, demonstrating uniform dark current across the array.

Keeping in mind that the ultimate goal of infrared detector work is to develop an IR imaging camera, we have attempted to image a heated object with a single device, which we refer to as single pixel imaging. This allows us to demonstrate imaging with QDIPs, even though we are still in the process of designing and fabricating large area focal plane arrays, which is an expensive and time-consuming endeavor. In order to conduct the measurement, we fabricated a 13x13 interconnected vertical QDIP array with a pixel diameter of 40  $\mu\text{m}$  and a pitch of 120  $\mu\text{m}$ . While this is not truly a single pixel, since a single average photocurrent is obtained from the entire array, the device behaves as a single pixel with a very large optical area. An X-Y pair of gold-coated mirrors servo-actuated by galvanometers is used to raster scan IR light from the object across the QDIP array. The mirror pair is mounted in a bracket whose exit window is the limiting aperture of the measurement. The QDIP array is mounted inside a cryostat with a KRS-5

window, and a lock-in amplifier is used for data acquisition. The object we chose to image is a graphite furnace igniter, which becomes red-hot when a wall current is passed through it. The image, obtained for a detector temperature of 80 K, is shown in figure 5. A very small section of the igniter is imaged due to the limiting aperture in the X-Y mirror bracket.

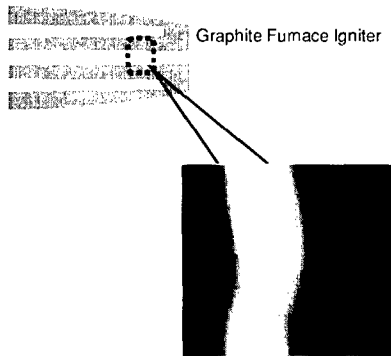


**Figure 5.** Raster-scanned single pixel image of a section of a graphite furnace igniter obtained at a detector temperature of 80 K for the vertical QDIP heterostructure with a single AlGaAs barrier.

## CONCLUSIONS

To conclude, the properties of a vertical InAs/GaAs QDIP with a single 30% AlGaAs barrier have been investigated. This device demonstrates very high  $D^*$  values and a high operating temperature for normal-incidence. This device is also unique in that its high performance at low bias demonstrates its suitability for incorporation in a focal plane array that uses commercially available silicon read-out circuits, as demonstrated by a dark current uniformity measurement across a 4x4 vertical QDIP array. The promise of using QDIPs for infrared detection is also demonstrated by the imaging of a heated object with a single interconnected QDIP array. While the low responsivity of these devices must be improved in order to further increase the performance of the QDIPs, their high temperature operation and initially favorable imaging properties certainly motivate further investigation and development.

## ACKNOWLEDGEMENTS

This work is being supported by ARO under Grants DAAD19-01-1-0462 and DAAD19-00-1-0394 (DARPA program).

## REFERENCES

1. K. W. Berryman, S. A. Lyon, and M. Segev, "Mid-infrared photoconductivity in InAs quantum dots," *Appl. Phys. Lett.*, 70, pp. 1861-1863, 1997.
2. J. Phillips, K. Kamath, and P. Bhattacharya, "Far-infrared photoconductivity in self-organized InAs quantum dots," *Appl. Phys. Lett.*, 72, pp. 2020-2022, 1998.
3. S. Kim, H. Mohseni, M. Erdtmann, E. Michel, C. Jelen, and M. Razeghi, "Growth and characterization of InGaAs/InGaP quantum dots for mid-infrared photoconductive detector," *Appl. Phys. Lett.*, 73, pp. 963-965, 1998.
4. S. Maimon, E. Finkman, and G. Bahir, "Intersublevel transitions in InAs/GaAs quantum dots infrared photodetectors," *Appl. Phys. Lett.*, 73, pp. 2003-2005, 1998.
5. D. Pan, E. Towe, and S. Kennerly, "Normal-incidence intersubband (In, Ga)As/GaAs quantum dot infrared photodetectors," *Appl. Phys. Lett.*, 73, pp. 1937-1939, 1998.
6. S. J. Xu, S. J. Chua, T. Mei, X. C. Wang, X. H. Zhang, G. Karunasiri, W. J. Fan, C. H. Wang, J. Jiang, S. Wang, and X. G. Xie, "Characteristics of InGaAs quantum dot infrared photodetectors," *Appl. Phys. Lett.*, 73, pp. 3153-3155, 1998.
7. Q. D. Zhuang, J. M. Li, H. X. Li, Y. P. Zeng, L. Pan, Y. H. Chen, M. Y. Kong, and L. Y. Lin, "Intraband absorption in the 8-12  $\mu\text{m}$  band from Si-doped vertically aligned InGaAs/GaAs quantum-dot superlattice," *Appl. Phys. Lett.*, 73, pp. 3706-3708, 1998.
8. A. Weber, O. Gauthier-Lafaye, F.H. Julien, J. Brault, M. Gendry, Y. Désieres, and T. Benyattou, "Strong normal-incidence infrared absorption in self-organized InAs/InAlAs quantum dots grown on InP(001)," *Appl. Phys. Lett.*, 74, pp. 413-415, 1999.
9. J. Phillips, P. Bhattacharya, S. W. Kennerly, D. W. Beekman, and M. Dutta, "Self-Assembled InAs-GaAs Quantum-Dot Intersubband Detectors," *IEEE J. Quantum Electron.*, 35, pp. 936-943, 1999.
10. L. Chu, A. Zrenner, G. Böhm, and G. Abstreiter, "Normal-incident intersubband photocurrent spectroscopy on InAs/GaAs quantum dots," *Appl. Phys. Lett.*, 75, pp. 3599-3601, 1999.
11. D. Pan, E. Towe, and S. Kennerly, "Photovoltaic quantum-dot infrared detectors," *Appl. Phys. Lett.*, 76, pp. 3301-3303, 2000.
12. H. C. Liu, M. Gao, J. McCafferey, Z. R. Wasilewski, and S. Fafard, "Quantum dot infrared photodetectors," *Appl. Phys. Lett.*, 78, pp. 79-81, 2001.
13. Y. Wang, S. D. Lin, H. W. Wu, and C. P. Lee, "Low dark current quantum-dot infrared photodetectors with an AlGaAs current blocking layer," *Appl. Phys. Lett.*, 78, pp. 1023-1025, 2001.
14. A. Rogalski, "Assessment of HgCdTe photodiodes and quantum well infrared photoconductors for long wavelength focal plane arrays," *Infrared Phys. & Technol.*, 40, pp. 279-294, 1999.
15. A. Rogalski, *Infrared Detectors*, pp. 155-650, Gordon and Breach Science Publishers, Australia, 2000.
16. B.F. Levine, "Quantum-well infrared photodetectors," *J. Appl. Phys.*, 74, pp. R1-R81, 1993.

17. S. D. Gunapala and K. M. S. V. Bandara, "Recent Developments in Quantum-Well Infrared Photodetectors," *Thin Films*, 21, pp. 113-237, 1995.
18. J. Singh, "Possibility of room temperature intra-band lasing in quantum dot structures placed in high-photon density cavities," *IEEE Photon. Technol. Lett.*, 8, pp. 488-490 , 1996.
19. D. Klotzkin, K. Kamath, and P. Bhattacharya, "Quantum capture times at room temperature in high-speed  $In_{0.4}Ga_{0.6}As$ -GaAs self-organized quantum-dot lasers," *IEEE Photon. Technol. Lett.*, 9, pp. 1301-1303, 1997.
20. J. Urayama, T. B. Norris, J. Singh, and P. Bhattacharya, "Temperature dependent carrier dynamics in InGaAs self-assembled quantum dots," *Phys. Rev. Lett.*, 86, pp. 4930-, 2001.
21. D. Klotzkin and P. Bhattacharya, "Temperature dependence of dynamic and dc characteristics of quantum dot and quantum well lasers: A comparative study," *IEEE J. of Lightwave Technol.*, 17, pp.1634-, 1999.
22. T. Sosnowski, T. Norris, H. Jiang, J. Singh, K. Kamath, and P. Bhattacharya, "Rapid carrier relaxation in  $In0.4Ga0.6As/GaAs$  quantum dots characterized by differential transmission spectroscopy," *Phys. Rev. B-Condensed Matter*, 57, pp. R9423-, 1998.
23. K. Mukai, N. Ohtsuka, H. Shoji, and M.Sugawara, "Emission from discrete levels in self-formed InGaAs/GaAs quantum dots by electric carrier injection: influence of phonon bottleneck," *Appl. Phys. Lett.*, 68, pp. 3013-, 1996.
24. A. D. Stiff, S. Krishna, P. Bhattacharya, and S. Kennerly, "High-detectivity, normal-incidence, mid-infrared ( $\sim 4 \mu m$ ) InAs/GaAs quantum-dot detector operating at 150 K," *Appl. Phys. Lett.*, 79, pp. 421-423, 2001.
25. A. D. Stiff, S. Krishna, P. Bhattacharya, and S. Kennerly, "Normal-Incidence, High-Temperature, Mid-Infrared, InAs/GaAs Vertical Quantum-Dot Infrared Photodetector," *IEEE J. of Quant. Electron.*, 37, pp. 1412-1419, 2001.